Polymer 49 (2008) 5564–5574

Contents lists available at ScienceDirect

Polymer

journal homepage: www.elsevier.com/locate/polymer

Carbon nanocapsules-reinforced syndiotactic polystyrene nanocomposites: Crystallization and morphological features

Chi Wang [a,*], Chien-Lin Huang [a], Yu-Chen Chen [a], Gan-Lin Hwang [b], Shih-Jung Tsai [b]

[a] Department of Chemical Engineering, National Cheng Kung University, Tainan 701, Taiwan, ROC
[b] Nano-Powder and Thin Film Technology Center, Industrial Technology Research Institute, Tainan 709, Taiwan, ROC

ARTICLE INFO

Article history:
Received 31 July 2008
Received in revised form
18 September 2008
Accepted 21 September 2008
Available online 9 October 2008

Keywords:
Syndiotactic polystyrene
Carbon nanocapsules
Morphology

ABSTRACT

Syndiotactic polystyrene (sPS) composites filled with well-dispersed carbon nanocapsules (CNC) were prepared through solution blending along with ultrasonication. Several analytic techniques, including DSC, FTIR, PLM, WAXD, TEM, and TGA were performed to reveal the CNC effects on the crystallization, morphology and the thermal degradation of the as-prepared sPS/CNC composites. Addition of CNC was found to favor the crystalline modification of β-form sPS and depress the α-form ones. For the dynamic crystallization, a gradual reduction of cold-crystallization temperature of the α-form sPS was observed by increasing the CNC content although the glass transition temperature remained unchanged (~96 °C). In contrast, the melt-crystallization temperature of the β-form sPS was elevated from 238 °C for the neat sPS to 251 °C for the 99/5 composite in spite of the fact that the equilibrium melting temperature (~290 °C) determined from the linear Hoffman–Weeks plot was irrelevant with CNC concentrations. The former was attributable to the formation of an effective heat-conduction path to trigger an earlier overall crystallization. On the other hand, the latter resulted from the enhanced nucleation sites due to the presence of uniformly dispersed CNCs. Results of the isothermal crystallization of the β-form sPS concluded that the presence of 1% CNCs led to a significant increase in the crystallization rate as much as an order of magnitude. Moreover, the Avrami exponent changed to ~2.0 from a value of 2.8 for the neat sPS, suggesting a different crystallization mechanism involved. At a given crystallization temperature, PLM results showed a negligible variation in the crystal growth rates and a decrease in spherulitic sizes, indicating that nucleation played the key role in enhancing the crystallization rate. For samples isothermally crystallized at 260 °C, the lamellar thickness was constant to be ~7.2 nm regardless of the CNC content. Due to the enhanced nucleation, however, lamellar stacks were more randomly oriented and its lateral dimensions became shorter with increasing CNC contents. For composites with more than 1 wt% CNC, the crystallizability of sPS chains was reduced and the annealing peak located ca. 4 °C higher than the crystallization temperature became more evident, suggesting the plausible formation of micro-crystals in between the lamellar stacks. The TGA results illustrated that a better thermal stability was reached for the CNC-filled sPS composites.

1. Introduction

Polymer composites containing nano-scaled fillers have been attracting much attention recently due to the wide-spread interest in the nanotechnology application. Among all the nano-scaled fillers, carbon nanotube (CNT) and its associated materials, such as C_{60} and carbon nanocapsules (CNC), are the most promising materials for the advanced application due to its excellent mechanical and electrical properties [1]. In contrast with CNT that possesses a high aspect ratio ($>10^2$), CNC is a special type of CNT with a much lower aspect ratio (1–2) [2–5]. Basically, CNCs are polyhedral nano-scaled particles that consist of a concentric grapheme-layered structure with a cavity in the center. CNCs are thermally stable up to 900 °C under an inert atmosphere. Syndiotactic polystyrene (sPS) is a relatively new material with unique properties, such as high melting temperature and good chemical resistance. This is in comparison with the other two isomers, i.e. atactic PS (aPS) and isotactic PS (iPS). sPS is a semi-crystalline polymer with a glass transition at ~95 °C and an apparent crystalline melting temperature at ~270 °C. Due to its polymorphic nature, at least four types of crystalline modifications (designated as α, β, γ and δ) have been identified depending upon the sample

* Corresponding author. Tel.: +886 6 2757575x62645; fax: +886 6 2344496.
E-mail address: chiwang@mail.ncku.edu.tw (C. Wang).

0032-3861/$ – see front matter © 2008 Elsevier Ltd. All rights reserved.
doi:10.1016/j.polymer.2008.09.057

preparation [6–16]. Mechanical strength and chemical resistance of sPS samples are associated with crystalline structure as well as crystallinity and their well-developed morphology. When induced from the melt state, either α- or β-form crystals with TTTT chain conformation can be obtained. In contrast, δ- and γ-form crystals with TTGG chain conformation are favored by solution crystallization when solvent is involved. Currently, there are many articles that have studied the characteristics of crystalline structure using wide-angle X-ray diffraction (WAXD) and Fourier transform infrared spectroscopy (FTIR) [14–16].

Effects of CNTs on the crystallization and morphologies of polymers have been investigated in many polymers such as polyethylene [17–19], polypropylene [20–25], poly(vinyl alcohol) [26] and poly(ethylene oxide) [27]. However, to the best of our knowledge, there are no reports of sPS crystallization induced by CNCs (or CNTs) to date. Two important issues should be addressed to prepare polymer composites with CNT nano-particles. The first is the requirement of uniform distribution of CNTs throughout the polymer matrix to provide effective reinforcement for either mechanical, heat or electric properties. The second is the presence of good interfacial strength between CNTs and polymers for transferring the applied load from the matrix to the CNTs. A modification of the CNT surface is generally required to achieve these two goals.

In this paper, we described the effects of CNC addition on the crystallization, crystalline modification, crystal growth rate, thermal stability and lamellar morphologies developed in the sPS/CNC composites using several analytical techniques. In contrast with sPS/CNC composites, CNTs are also employed as the counterpart filler to reveal the aspect ratio of carbon tubes on the crystallization kinetics of sPS. Our results show that both CNCs and CNTs are excellent nucleating agents to enhance the crystallization rate of sPS matrix.

2. Experimental

2.1. Materials and composite preparation

sPS pellets with a weight average molecular weight of 200 kg/mol were obtained from Dow Chemical Co. CNCs and CNTs were kindly provided by ITRI. The densities of sPS and CNC are 1.06 and 1.60 g/cm^3, respectively. According to ITRI, CNCs were produced by a pulse plasma arc-discharge method [3]. The as-received CNCs were dispersed in the H_2SO_4/HNO_3 solution with a weight ratio of 3/1 in an ultrasonic bath at room temperature for 1 h so as to modify the CNC surface and then were refluxed at 80 °C for 6 h to induce –COOH group upon the CNC particles. After filtration, the CNC particles were collected and rinsed with deionized water until the PH of mixture reached 7. Later, they were dried at 75 °C prior to the composite preparation. Similar surface treatments were performed for the as-received CNT particles.

sPS/CNC composites with various compositions were prepared by dissolving the weighted sPS pellets in *ortho*-dichlorobenzene (*o*-DCB) solvent at 140 °C, and the surface-treated CNCs were then added to the homogeneous solution. This was followed by ultrasonic treatment for 3 h. The uniform solution suspension with 1% (w/v) was then precipitated drop-by-drop into a 20-fold excess volume of methanol. The precipitated composite powders were continuously dried in a vacuum oven until the residual solvent was removed. This was subsequently judged from the FTIR spectra in the absence of any *o*-DCB absorbance peaks at 1130, 1170 and 1249 cm^{-1}. The as-prepared composites exhibited a small IR absorbance peak at 572 cm^{-1}, and WAXD results showed the diffraction angles at 9.2°, 15.9° and 17°(Cu target), indicating the presence of small amount of γ-form crystallites [28]. Composites with CNC weight fractions ranging from 0.001 to 0.05 were prepared in this manner. In this work, the code of 99/1 represents the weight ratio of sPS to CNC, and the corresponding volume fraction (ϕ_{CNC}) is obtained using the respective densities of sPS and CNC.

2.2. DSC measurements for crystallization kinetics

The crystallization and melting behavior of the sPS/CNC composites were investigated using a Perkin–Elmer DSC7 under N_2 atmosphere. Prior to measurements, indium and zinc standards were used to calibrate the enthalpies of fusion and melting temperatures. By holding the as-prepared samples at 300 °C for 10 min and then quenching in the liquid nitrogen, amorphous composites verified by FTIR and WAXD were obtained for the dynamic crystallization studies.

To perform the dynamic crystallization, the melt-quenched amorphous composites were heated at a rate of 10 °C/min to 300 °C for the cold-crystallization study (1st heating scan). After holding at 300 °C for 10 min, they were then cooled at a rate of 10 °C/min to room temperature for the melt-crystallization study (1st cooling scan). Afterwards, a subsequent heating at 10 °C/min was carried out to reveal the melting of sPS crystals developed during melt crystallization (2nd heating scan). To reveal the crystal modification developed in cold crystallization, in situ FTIR measurements were performed during 1st heating scan until melting. In addition, the crystal modification developed after melt crystallization was also studied by FTIR prior to the 2nd heating scan.

For isothermal crystallization, as-prepared samples were first held at 300 °C for 10 min to remove the thermal history. By this thermal treatment, our FTIR results showed that the memory effect of α-form crystallites was completely erased [8]. Samples were then rapidly cooled to the desired crystallization temperature (T_c) to complete the phase transformation, and a subsequent heating trace was performed at a heating rate of 10 °C/min. The crystallized samples were frequently checked by FTIR and WAXD and only β-form sPS crystallites were obtained for samples crystallized in this manner.

2.3. FTIR measurements for crystal modification

In situ FTIR measurements were performed using a Perkin–Elmer FTIR spectrometer (Spectrum 100) equipped with a Mettler heating stage (FP900) for temperature control. In order to measure the instantaneous spectral changes during cold crystallization (1st heating scan), a resolution of 2 cm^{-1} with three scans were taken during heating at a rate of 10 °C/min. Consecutive spectral recording was performed at an interval of ~20 s until sample melting. On the other hand, a total of 32 scans with a resolution of 2 cm^{-1} were taken at room temperature for the melt-crystallized samples.

2.4. PLM measurements for crystal growth rate

A polarized light microscope (PLM, Leica DMLP) equipped with a hot stage (THMS600, Linkam) was used to monitor the dimension variation of spherulites (or axilites). The samples were first maintained at 300 °C for 10 min and then quickly cooled to T_c for crystallization. Crystal growth rate (G) of sPS was determined from the slope of spherulitic radius (or axilitic half-axis) versus elapsed time.

2.5. WAXD measurements for crystal modification

To characterize the crystal form of the sPS/CNC composites, WAXD intensity profiles of the crystallized samples were obtained using a DMAX2000 goniometer (Rigaku, Cu target). Data were collected from 5° to 30° in 2θ in steps of 0.02° at a scanning rate of 1°/min.

2.6. TEM observations for CNC dispersion and lamellar morphology

The ultrathin films, ca. 50 nm thick, were prepared by sectioning the bulk samples at room temperature using an Ultracut UCT (Leica) microtome. The particle size and dispersion of CNCs in the samples were observed using a transmission electron microscope (TEM, Jeol JEM-2000FX) operated at 80 kV. Staining of the ultrathin films was required to enhance the contrast between amorphous and lamellar layers. This was done to reveal the morphology of sPS lamellae. Sample staining was performed using ruthenium tetraoxide (RuO_4) vapors at room temperature.

2.7. TGA measurements for thermal stability

Thermo-gravimetric analysis (TGA) was performed on a TGA 2050 (TA instrument) apparatus under nitrogen flow (90 mL/min) from 50 to 800 °C at a heating rate of 10 °C/min. The weight of samples used was ~5 mg. The degradation temperature (T_d) was defined as the temperature at which the weight loss reached 5%.

3. Results and discussion

Filler dispersion is an important issue in characterizing the composite performance. Surface-treated CNCs (or CNTs) in the *o*-DCB solution exhibit good suspension after ultrasonic treatments [17,18]. Drop-wise co-precipitation of the sPS/CNC solutions from methanol essentially leads to composites with fair CNC dispersion under TEM bright field observations. Fig. 1a shows the typical TEM micrographs for the sPS/CNC = 95/5 composites in the absence of RuO_4 staining. The dark spots are the CNC particles. In addition to the primary CNC particles with a diameter of ~50 nm (inset), some agglomerates with a long axis of 400 nm and short axis of 200 nm are observed. Owing to the arc process condition, moreover, it should be noted that in addition to the CNC products some short CNTs with an aspect ratio less than 10 are occasionally produced [3]. The estimated amount of short CNT is less than 2 wt% in each batch. For the sPS/CNT composites, the CNTs used are the multi-walled CNT with an inner and outer diameter of ~6.7 and 20 nm, respectively. Fig. 1b shows the deposited CNTs structure on the TEM grid prepared from *o*-DCB solution with the inset showing the morphological feature of a single CNT. Generally speaking, the curvy CNTs are uniformly distributed although some small CNT agglomerates still inevitably persist due to the concentration increase of CNT during *o*-DCB evaporation [18].

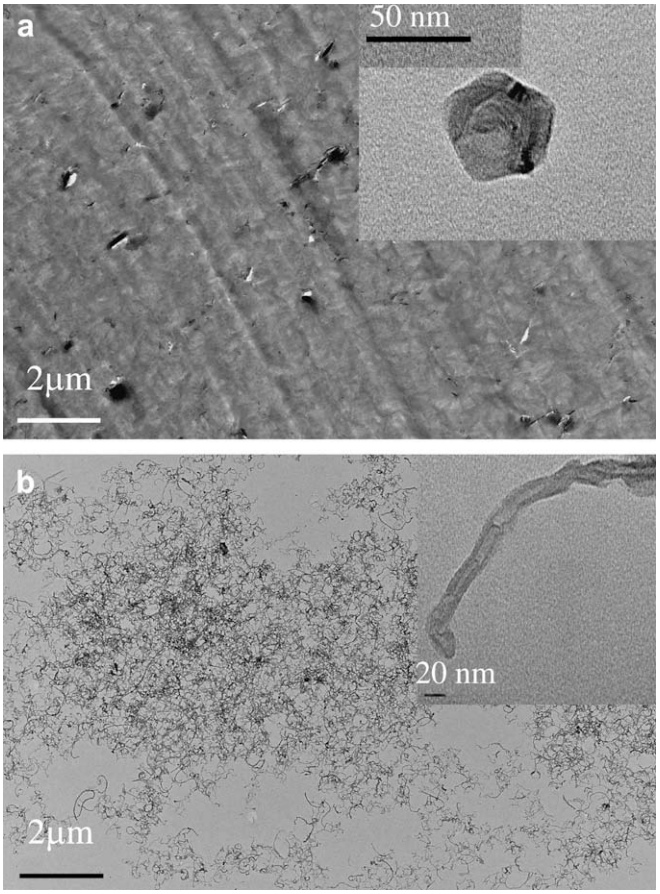

Fig. 1. TEM micrographs of (a) sPS/CNC = 95/5, the sample is not stained with RuO_4 vapor in order to reveal more clearly the location of CNC primary particles and CNC agglomerates; the inset shows the primary CNC particles with a diameter of ~50 nm, (b) CNT dispersion in the *o*-DCB solution; the inset shows a single curvy CNT with a outer diameter and inner diameter of 20 and 6.7 nm, respectively.

3.1. CNC effects on the crystal modification of sPS

Neat sPS exhibits two possible crystalline structures when crystallized from the melt state. These are the α- and β-forms, depending upon the thermal treatments. It is generally accepted that β-form is thermodynamically more stable, whereas α-form is meta-stable and is favored by a kinetic crystallization path. Based on an extensive WAXD study, De Rosa et al. [8] attributed the formation of α-form to a memory effect. Two key factors are crucial, i.e. the melt holding temperature (T_{max}) and the residence time at that temperature (t_{max}), in determining the final crystalline structure of sPS samples. Higher T_{max} and larger t_{max} lead to the memory erase of the α-form and give rise to the preferential production of β-form. To reveal the effect of CNC addition on the sPS crystal form, we carried out FTIR measurements to characterize the melt-crystallized samples, which were maintained at various T_{max} for 10 min and then cooled at a rate of 10 °C/min to room temperature. Fig. 2 shows the typical FTIR spectra for samples with T_{max} of 275 °C. The absorbance peaks at 858 and 911 cm^{-1} are associated with the β-crystalline form, whereas 852 and 902 cm^{-1} are relevant with

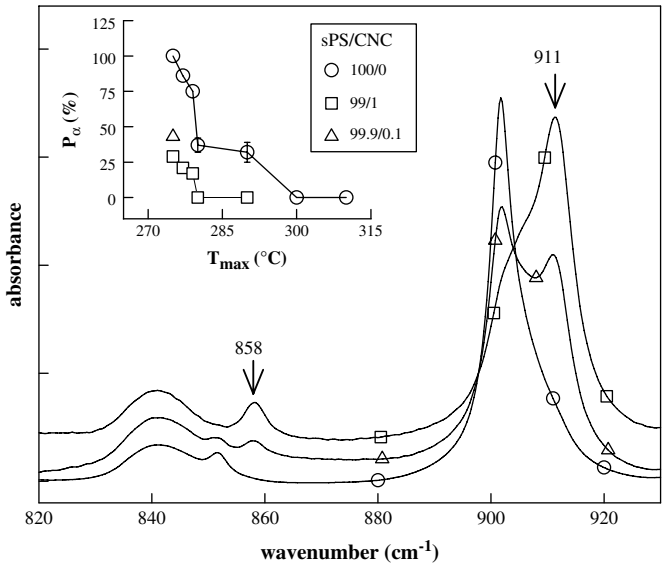

Fig. 2. FTIR spectra of as-prepared sPS/CNC samples held at 275 °C for 10 min and cooled to room temperature at a rate of 10 °C/min. The characteristic absorbance peaks for β-form sPS are 858 and 911 cm^{-1} (arrows), and those for α-form are 852 and 902 cm^{-1}. The inset shows the content of α-form crystallites (P_α) developed in the samples after being held at T_{max} for 10 min prior to 10 °C/min cooling to room temperature.

the α-crystalline form. In the respective wavenumber region, the absorbance band contributed from the amorphous phase is located at 841 and 906 cm^{-1}, respectively. It is apparent that only α-crystalline form is observed for the neat sPS sample; however, a small amount of CNC addition leads to the favorite formation of the β-crystalline form. Wu et al. [16] have derived an empirical equation to estimate the percentage of α-form (P_α) developed in the crystallites, as follows,

$$P_\alpha = \frac{A_{852}/a_\alpha}{A_{852}/a_\alpha + A_{858}/a_\beta} \quad (1)$$

where A_{841}, A_{852}, and A_{858} are the integrated area of amorphous, α- and β-forms, respectively, after de-convolution of the spectra ranging from 865 to 820 cm^{-1}. The conversion coefficient a_α and a_β are found to be 0.178 and 0.272, respectively. Based on Eq. (1), the T_{max} dependence of P_α is shown in the inset of Fig. 2. It should be noted that the as-prepared composites, mainly in the amorphous state, will preferentially crystallize in the α-form and are subsequently melted away during heating to T_{max} (Fig. 3a, discussed later). For the neat sPS sample, T_{max} of 300 °C is sufficiently high to erase all the α-form memory, producing crystallites with β form only. For T_{max} lower than 300 °C, on the other hand, mixed α/β-crystalline form is found and the α-form content is gradually increased with decreasing T_{max}. At $T_{max} = 275$ °C, only α-form crystallites are obtained in the absence of β form. With respect to the T_{max} dependence of P_α, our FTIR results are consistent with those based mainly on the WAXD results [8,29]. Addition of CNC leads to the reduction of P_α at a given T_{max}, and the transition for the full β-form formation is significantly decreased to 277 °C for the sPS/CNC = 99/1 composites. Our FTIR results indicate that formation of β-form sPS is favored after the adding CNC particles. Previous findings on the polymorphism issue demonstrated that addition of foreign particles (clays [30,31] and nano-$CaCO_3$ [29]) or miscible polymers (aPS [32], poly(styrene-*co*-α-methyl styrene [33], and poly(2,6-dimethylphenylene) [32,34]) seem to favor the β-form and depress the α-form formation.

3.2. Dynamic crystallization

For the melt-quenched amorphous composites, the heating traces are shown in Fig. 3a. T_g is measured from the mid-point of the heat capacity jump; the peak temperature of the cold crystallization is referred to as $T_{p,cc}$, and the crystallization enthalpy determined from the integral area of the exotherm is denoted ΔH_{cc}. Based on the in situ FTIR measurements, the crystallites developed are in the α-form regardless of the CNC content (Fig. 4). Therefore, the melting temperature is referred to as $T_{m,\alpha}$. For the melt crystallization studies, the samples were held at 300 °C for 10 min and were then cooled down at a rate of 10 °C/min. Fig. 3b shows the cooling curves with the crystallization peak temperature and exothermic enthalpy denoting $T_{p,mc}$ and ΔH_{mc}, respectively. Moreover, the FTIR spectra of the melt-crystallized samples show the exclusive presence of β-form sPS (Fig. 5). Thus, the subsequent heating scan (Fig. 3c) displays the melting of β-form sPS, and the corresponding melting temperature is denoted to $T_{m,\beta}$. The measured thermal properties are tabulated in Table 1, in which ΔH_{cc} and ΔH_{mc} are normalized with ϕ_{CNC} to represent its crystallizability owing to the presence of CNCs.

Fig. 4 shows the FTIR spectral changes of neat sPS samples during cold crystallization; similar spectra are obtained for the other CNC-filled composites and the results are not shown for brevity. The absence of 911 cm^{-1} absorbance peak suggests the exclusive formation of α-form sPS during 1st heating scan. Cold-crystallization process is recognized by the increase of the integrated area of 1222 cm^{-1} peak (A_{1222}), accompanying with a gradual band shift from 906 to 903 cm^{-1}. Further band shift takes place during heating to 901.5 cm^{-1} prior to crystal melting at ~250 °C, at which spectral recording becomes infeasible due to the

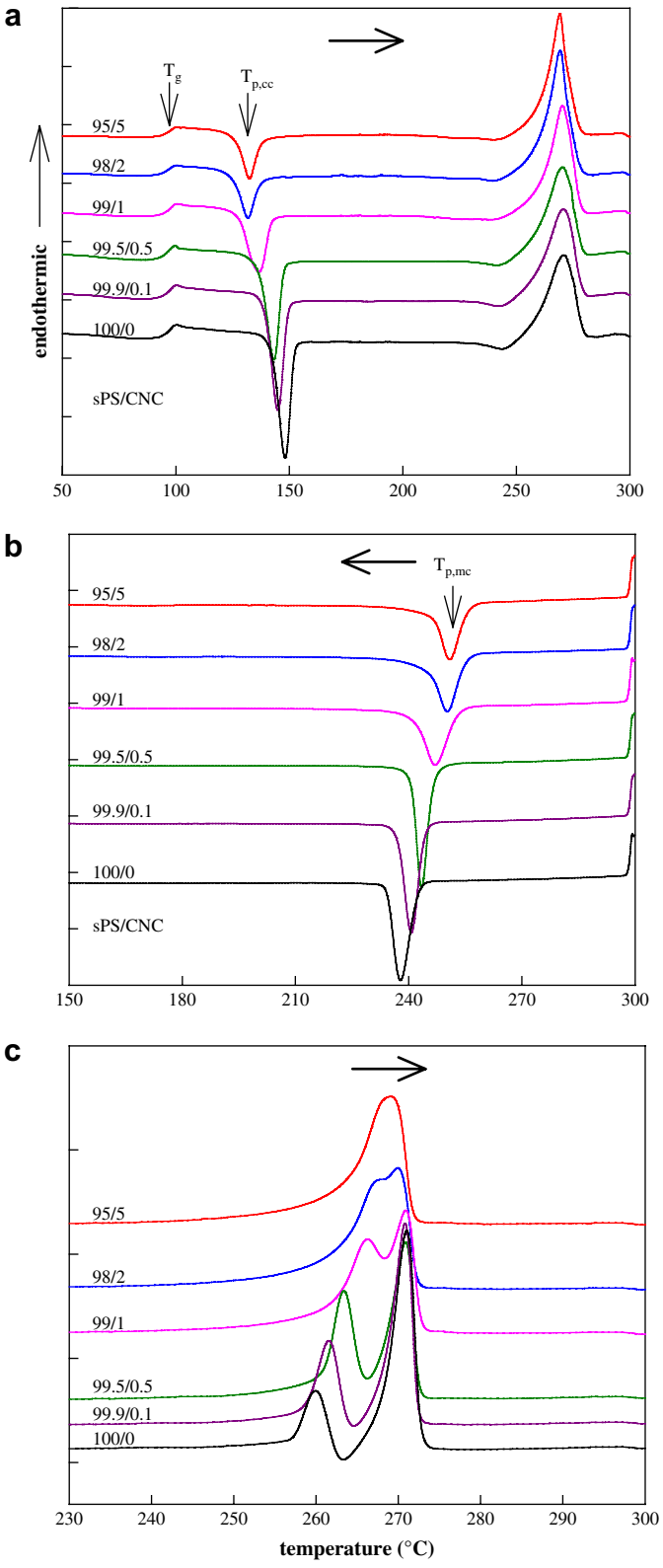

Fig. 3. (a). DSC heating traces recorded for neat sPS and sPS/CNC composites for cold crystallization studies. The melt-quenched amorphous samples are heated at 10 °C/min to 300 °C. (b) DSC cooling for neat sPS and sPS/CNC composites for melt crystallization studies. After holding at 300 °C for 10 min, the samples are cooled at 10 °C/min to room temperature. (c) Subsequent heating at 10 °C/min after (b).

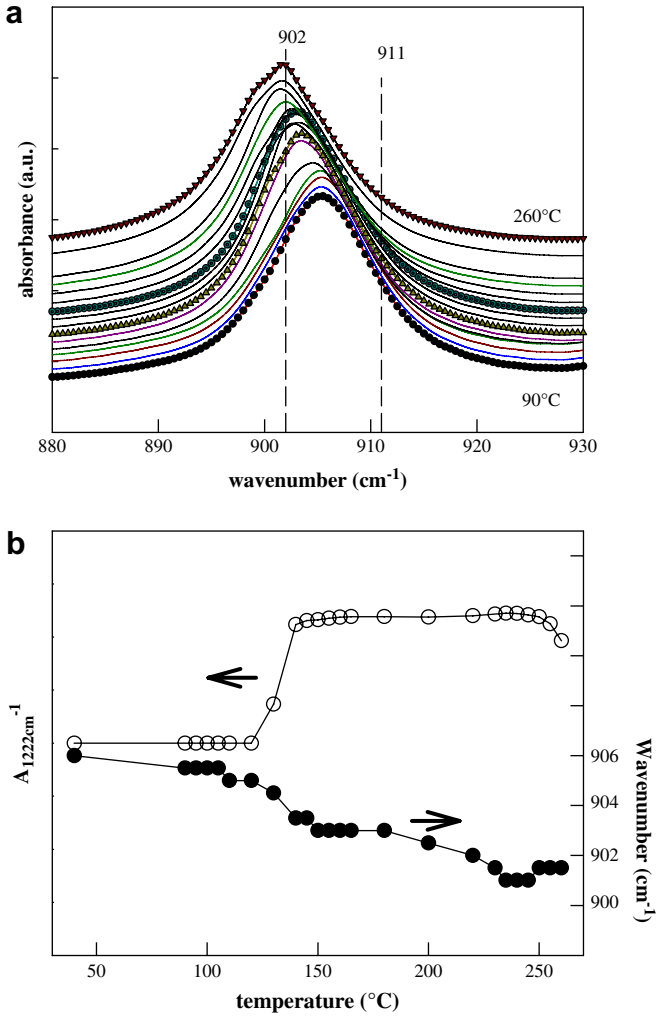

Fig. 4. (a). In situ FTIR spectra for the amorphous 100/0 sample during heating from 90 to 260 °C, (b) variation of absorbance peak and the integrated area of 1222 cm^{-1} band (A_{1222}) with temperature. Heating rate: 10 °C/min.

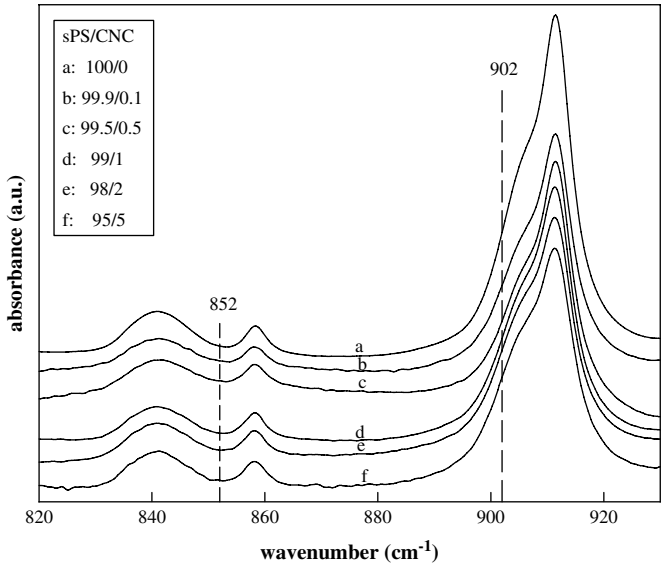

Fig. 5. FTIR spectra of dynamically melt-crystallized samples to reveal the crystal modification developed.

Table 1
Thermal properties of sPS/CNC composites obtained from the dynamic cold and melt crystallization.

sPS/CNC	T_g (°C)	$\Delta H_{cc}/(1-\phi_{CNC})$ (J/g)	$T_{m,\alpha}$ (°C)	$\Delta H_{mc}/(1-\phi_{CNC})$ (J/g)	$T_{m,\beta}$ (°C)
100/0	96.62 ± 0.03	15.97 ± 0.27	270.5 ± 0.3	26.54 ± 0.01	260.2/271.1
99.9/0.1	96.52 ± 0.16	15.63 ± 0.61	270.5 ± 0.1	26.65 ± 0.26	263.1/271.4
99.5/0.5	95.63 ± 0.41	15.02 ± 0.34	271.0 ± 0.8	26.75 ± 0.28	263.6/271.1
99/1	96.40 ± 0.40	12.30 ± 0.72	270.3 ± 0.2	25.18 ± 0.17	266.1/270.8
98/2	96.47 ± 0.50	7.57 ± 0.60	269.8 ± 0.7	24.92 ± 0.40	270.2
95/5	96.64 ± 0.20	6.87 ± 0.37	269.3 ± 0.2	23.41 ± 0.57	269.3

sample flow. For the kinetics of cold crystallization, consistent results can be obtained between DSC and in situ FTIR measurement. As the amount of CNC is increased, T_g remains relatively unchanged at ~96 °C (Table 1). $T_{p,cc}$ is gradually shifted to a lower temperature together with the reduction of sPS crystallizability when ϕ_{CNC} is larger than 1%. The constant T_g indicated that no specific interaction between the surface-modified CNCs and the non-polar sPS chains. However, acid treatment on the CNCs (and CNTs) is believed to provide a better suspension status during blending with sPS chains in the *o*-DCB solution. As shown in Fig. 3a, a single melting peak

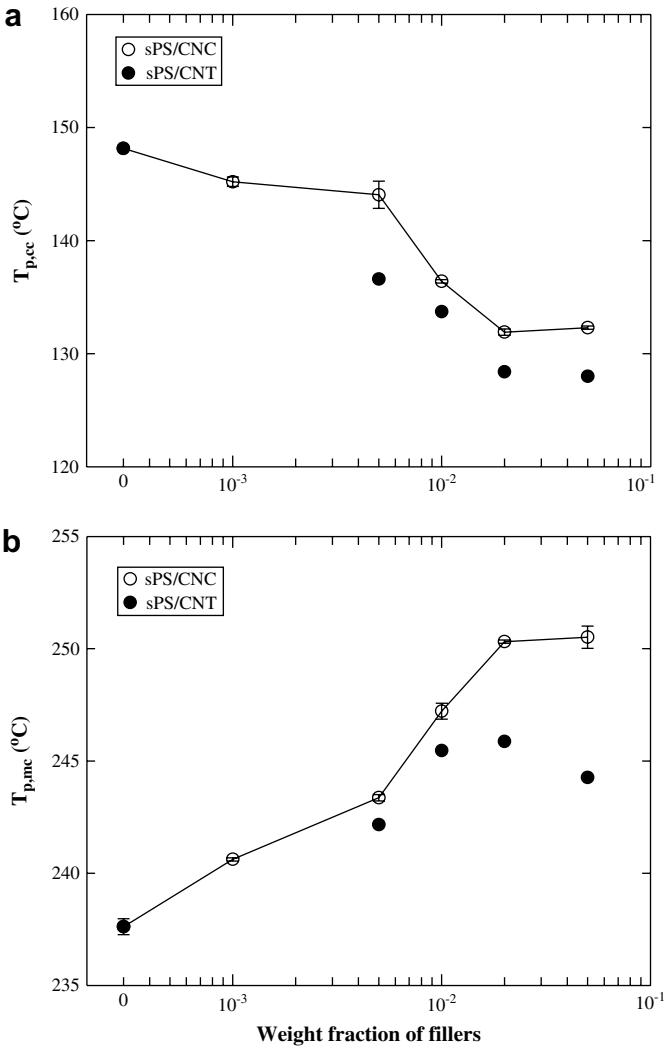

Fig. 6. Effects of CNC and CNT content on the (a) cold-crystallization temperature and (b) melt-crystallization temperature. Solid symbols are for the sPS/CNT composites to reveal the aspect ratio effect of carbon nanotubes.

located at a temperature of ca. 270.4 °C is seen for the cold-crystallized samples irrespective of the CNC content. Similar results were reported for the sPS/aPS blend system [35]. From the thermodynamic point of view, both T_g and T_m are important parameters in charactering the crystallization process. The former determines the lower bound temperature and indicates the level of chain mobility which is predominant for the cold crystallization. Conversely, the latter gives the upper bound temperature and is crucial for the nucleation process for the melt crystallization. The decrease in $T_{p,cc}$ implies a promoted process for sPS cold crystallization, which could be due plausibly to the enhanced chain mobility. However, as the T_g is practically unchanged after CNC incorporation, the enhancement of cold crystallization must be attributed to a better heat conduction owing to the presence of CNC particles, which activate the crystallization at a lower temperature. As shown in Fig. 6a, the aspect ratio of carbon tubes does play an important role in inducing crystallization of sPS. CNTs exhibit a more effective reduction of $T_{p,cc}$ due to its network formation for heat conduction in comparison with CNCs. Indeed, the high aspect ratio of CNT allows the formation of a percolated structure for heat transfer at very low volume contents (Fig 1b). A theoretical consideration of well-dispersed cylindrical fillers with an aspect ratio of 10^3 predicts only 0.05 vol.% fillers required to develop the percolation structure [36]. It is noted that $T_{p,cc}$ is leveled off at a filler content of 2 wt% and the $T_{p,cc}$ reduction can be as high as 16 and 20 °C for the CNC- and CNT-filled composites, respectively.

For the melt crystallization, on the other hand, $T_{p,mc}$ is shifted to a higher temperature (Fig. 3b) and the normalized ΔH_{mc} is apparently decreased for a given ϕ_{CNC} larger than 1 wt% (Table 1). The measured values of $T_{p,mc}$ of sPS/CNT composites are also shown for comparison in Fig 6b. The effect is less pronounced than CNC addition despite the addition of CNTs also causes an increase in the rate of melt crystallization. This may be attributed to the difference in the filler dispersion. The CNCs with a lower aspect ratio are likely to disperse more uniformly throughout the samples than the CNTs, which may readily form agglomerates. Thus, more effective (primary) nucleation sites are produced in the sPS/CNC composites to activate and accelerate the crystallization process for any given filler content. In contrast with the cold crystallization results (Fig. 3a), T_m of the melt-crystallized samples is increased with increasing CNC content (Fig. 3c). Melt-crystallized samples with ϕ_{CNC} lower than 1 wt% always exhibit dual melting peaks, whereas a single but broad melting peak is observed for composites with higher CNC content. In other words, the low melting peak gradually moves to a high temperature and is eventually merged with the high melting peak when ϕ_{CNC} is 2 wt% or larger. It should be noted that β-form sPS is favored when samples are dynamically crystallized from the melt state (Fig. 5). Due to the elevation of $T_{p,mc}$ (Fig. 3b), composites with a higher CNC content will experience a lower supercooling degree as the equilibrium melting temperature (T_m^0) of the β-form crystals remains intact (as discussed later). This in turn produces thicker lamellae that are melted away at a higher temperature during heating.

In a short summary for the dynamic crystallization, the addition of CNCs up to 1 wt% is found to render a sharp reduction of $T_{p,cc}$ as well as a significant elevation of $T_{p,mc}$. In comparison with those of neat sPS, the variation degree is ca. 12 and 10 °C, respectively. The present findings of CNC effects exhibit a distinct difference from those for the miscible sPS/aPS blends [35]. A negligible variation of T_g was also found with an increasing aPS content. However, $T_{p,cc}$ was shifted to higher temperatures and $T_{p,mc}$ was gradually reduced to lower temperatures. Both of these indicate the retardation of sPS crystallization induced either from the glass or from the melt. In other words, the addition of aPS leads to the dilution of crystallizable sPS chains and eventually retards the crystallization rate of sPS. This is in contrast with the effects of CNT incorporation found in the present study.

3.3. Isothermal crystallization

After obtaining the isothermal crystallization curves at a given T_c, the crystallization kinetics was studied using the Avrami equation as expressed by Eq. (2),

$$1 - X(t) = \exp\left[-k(t - t_i)^n\right] \quad (2)$$

where $X(t)$ is the relative crystallinity, t_i and t are the induction time and crystallization time, respectively, n is the Avrami exponent, and k is the overall crystallization rate. Based on Eq. (2), by plotting the $\ln[-\ln(1 - X(t))]$ versus $\ln(t - t_i)$ the initial slope gave the exponent n and value of k was deduced from the intercept. Fig. 7 shows the derived values of k and n for sPS/CNC composites at different T_c. The crystallization rate is reduced at high T_c for all the samples studied and addition of CNCs leads to the enhancement of sPS crystallization. An order of magnitude increase in k is found for the composites with 1 wt% CNCs. It is of interest to note that the derived Avrami exponent changed from ~2.8 for composites with

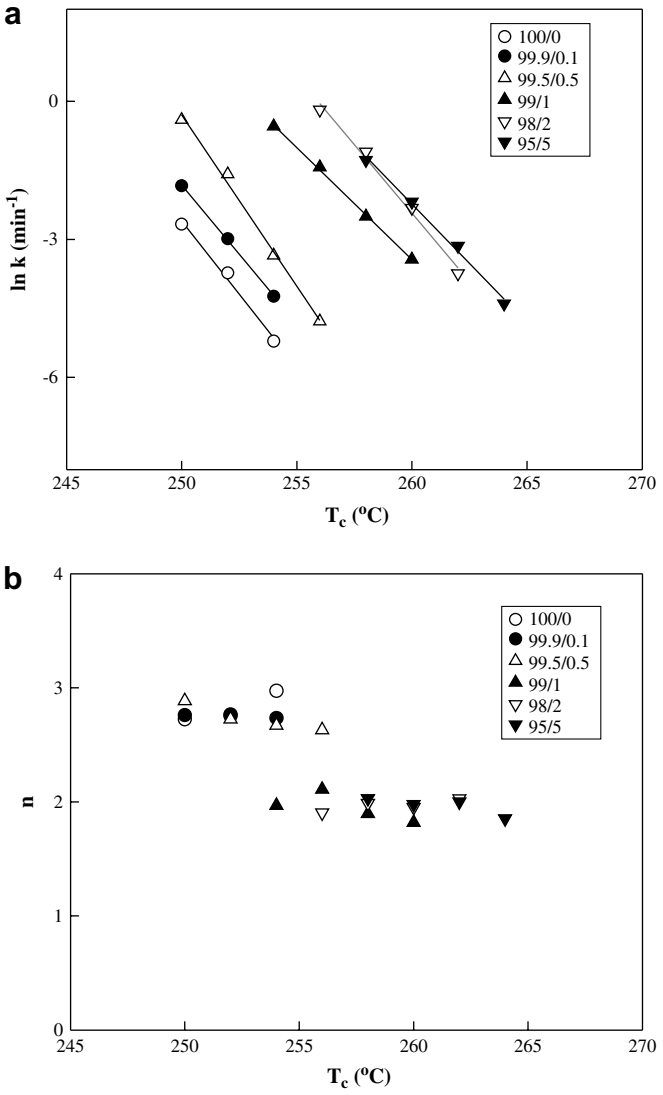

Fig. 7. Effects of crystallization temperature and CNC content on the (a) overall crystallization rate, k, (b) Avrami exponent, n.

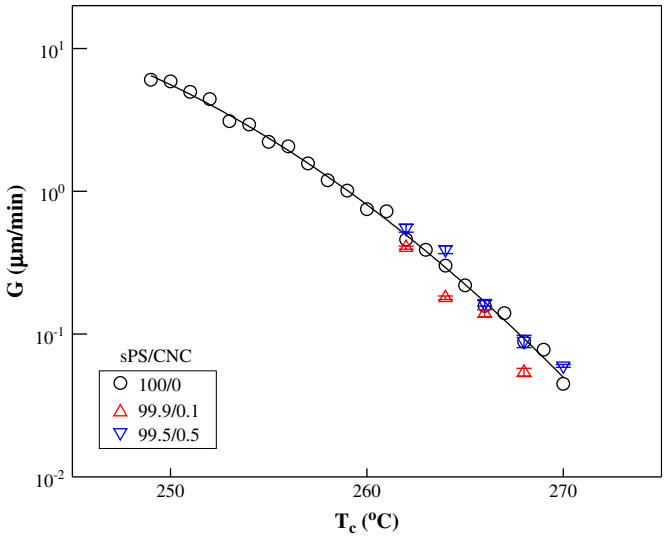

Fig. 8. Crystal growth rates of neat sPS and sPS/CNC composites.

less CNCs to ~2.0 for those with CNC contents higher than 0.5 wt%, suggesting a distinct variation of the nucleation and growth mechanism. At a given T_c, the increase in k by CNC addition could result from two possible events. The first is the enhanced nucleation density while the other is the increase in the crystal growth rate. The T_c dependence of crystal growth rate is shown in Fig. 8 to distinguish one from the other. Moreover, the PLM micrographs of samples crystallized at 256 °C are provided in Fig. 9. Apparently CNC fillers exhibit a negligible effect on the measured crystal growth rate. However, a pronounced decrease in the size of sPS spherulites is observed. For composites with CNC content more than 1 wt%, G measurements became infeasible due to the dense population of nuclei. For composites with CNC content lower than 0.5 wt%, either sPS spherulites or axilites can be identified. This is consistent with the derived Avrami exponent (~2.8), suggesting the heterogeneous nucleation together with three dimensional growth. Further increasing CNC content to 1 wt% leads to a significant increase in the nucleation density, accompanied with a reduced Avrami exponent to ~2.0, implying a two-dimensional growth mechanism. In fact, the over-crowded nuclei will accelerate the crystallization rate and produce more irregular crystalline lamellae as seen by TEM (discussed later). Thus, some crystallizable chains (or segments) might be trapped between these growth-restricted lamellae. This gives rise to the reduction of sPS crystallizability that is also observed in the isothermally crystallized samples. On studying the isothermal crystallization of sPS/clays composites, Wu et al. [37] also found a decrease of the Avrami exponent from ~2.5 for neat sPS to ~2.0 for 5 wt% clay in the temperature range of 255–263 °C. The introduction of 5 wt% clay into the sPS matrix significantly increased the overall crystallization rate due to the enhancement of nucleation. Similar CNT effects on the melt crystallization of polyethylene have been provided by Haggenmueller et al. [17]. They showed that Avrami exponent varied from ~2.7 for neat PE to ~1.6 for 1 wt% composite. Moreover, a tremendous increase in k (ca. five order magnitude) was obtained by adding only 1 wt% CNT. For the PP/CNT composites, previous reports [21,23] showed that k was increased with increasing CNTs but Avrami exponent was practically unchanged. Regarding the CNT effects on the matrix crystallization, all the collected results revealed that CNTs (or CNCs) can significantly enhance the heterogeneous nucleation to increase the crystallization rate. It is likely that nano-sized CNTs act like the conventional micro-scaled fibers to be able to induce transcrystallinity upon its surface by a preferential nucleation route. It is extremely difficult, if not impossible, for the bulk sample to readily observe the

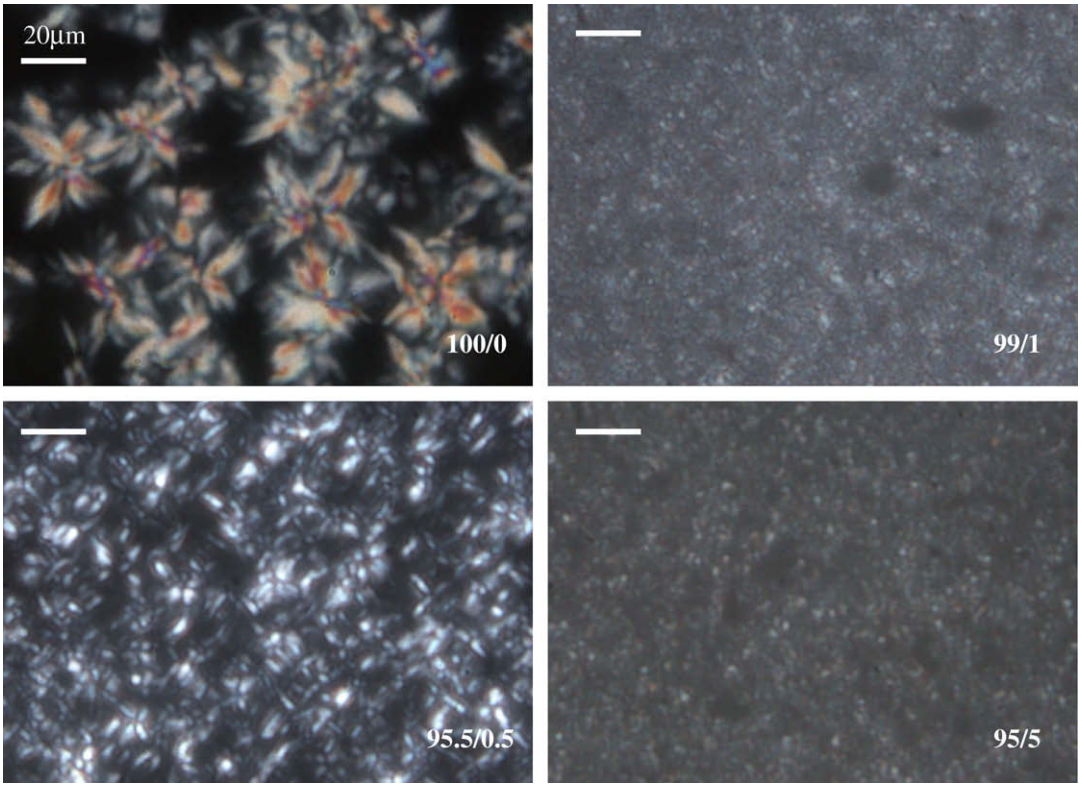

Fig. 9. PLM micrographs of sPS/CNC composites crystallized at 256 °C. The scale bar is 20 μm.

crystalline lamellae of matrix polymer in the vicinity of CNTs because the tube diameter is very small and sample staining is generally required for a better observation of lamellae. Using a coagulation process, Zhang et al. [25] prepared CNT fibers with a diameter of 40 μm from the polypropylene glycol solution containing CNTs with an average of 10 nm diameter and 1.0 mm length. These micron-sized CNT fibers were the first evidence to demonstrate its ability to develop PP transcrystallinty on its surface. However, it should be noted that the as-prepared CNT fibers essentially possessed a rough "fiber surface" (Fig. 2a, Ref. [25]) which might preserve the residual nuclei surviving at the melt temperature for the later crystallization. Up to recently, the nucleation ability of individual CNT is clearly "seen" under TEM observations on the basis of solution crystallization. It exhibited a shish-kebab-like structure with PE lamellae as the kebab growing perpendicularly to the shish CNT [18,19]. Based on the "size-dependent soft epitaxy" concept, many PE segments, with their chains parallel to the CNT axis, are deposited along the CNT surface to serve as the nucleation sites for later chain folding to develop PE kebab. Similar morphologies with CNT shish were provided from the Nylon 66/glycerin solution [19]. It is important to note that the shish CNTs are decorated periodically with the crystalline kebab by a distance as small as 20 nm. This suggested that CNTs (and CNCs) may provide profound nucleation sites under appropriate conditions to serve as an excellent nucleating agent. In accordance with the transcrystallinity developed upon the conventional fibers, similar features have been observed for the CNT-filled semi-crystalline composites except the "fiber-size" difference. Based on the WAXD and small-angle X-ray scattering, Haggenmueller et al. [17] calculated the *c*-axis orientation factor of PE crystals in the presence of CNTs and provided the supporting evidence for the formation of transcrystalline lamellae. That is to say CNTs template the crystallization of PE not only in the dilute solution but also in the melt state. Similar nucleation mechanism may develop in the present sPS/CNC composites, resulting in the change of crystal growth from three- to two-dimensions as indicated by the change of the Avrami exponent (Fig. 7b).

Fig. 10a shows the melting behavior of sPS/CNC = 95/5 composites after being completely crystallized at various T_c. The effects of CNC content on the melting behavior of composites melt-crystallized at 256 °C are displayed in Fig. 10b. Fig. 10a shows three melting peaks that were detected for samples that were crystallized at 244 °C. They are denoted by T_a, T_{ml} and T_{mh} from low to high temperatures. As T_c increases, T_{ml} is gradually shifted to a higher temperature and is eventually merged with T_{mh}. However, T_{mh} is independent of T_c. Moreover, T_a is always observed right above T_c and becomes more obvious at high T_c. Similar T_c effects have been observed in the other sPS/CNC composites. According to Fig. 10b, the appearance of T_a is more obscured for composites with less CNC content. A barely seen T_a is detected for the neat sPS sample.

The equilibrium melting temperature T_m^0 is the most important parameter for a crystallizable polymer because its crystallization kinetic is strongly related to the supercooling degree, ΔT defined by $T_m^0 - T_c$. To determine T_m^0, Hoffman–Weeks equation is frequently applied and expressed as follows [38],

$$T_m = T_m^0(1 - 1/\gamma) + T_c/\gamma \quad (3)$$

where T_m is the observed melting temperature of a crystal developed at a temperature of T_c, and γ is the thickening coefficient. Based on Eq. (3), a linear extrapolation of observed T_m as a function of T_c interests the $T_m = T_c$ line at a point, which provides the value of T_m^0. Fig. 11 shows the T_c dependence of melting peak temperatures for sPS/CNC composites. It is noted that regardless of the different CNC contents all composites show a superposition of the measured T_a, T_{ml} and T_{mh} and each master curve can be constructed. This

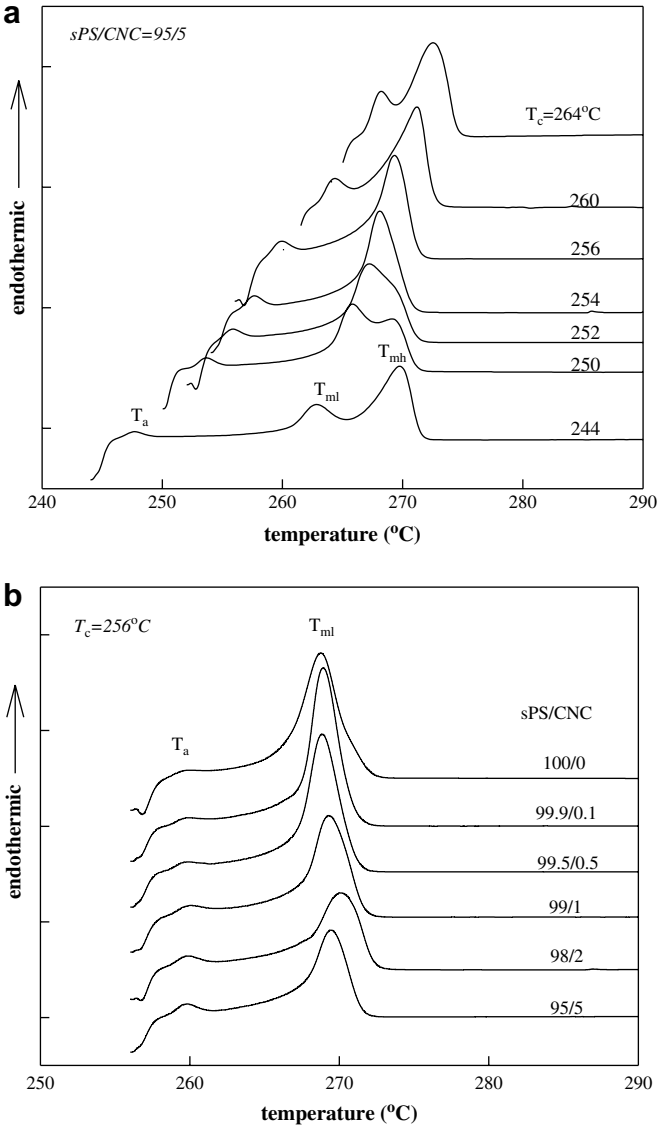

Fig. 10. Melting behavior of (a) 95/5 composites crystallized isothermally at various T_c, (b) different composites crystallized isothermally at 256 °C. Heating rate: 10 °C/min.

suggests that CNC addition plays no influence on the melting of crystalline lamellae, and the lamellar thickness may remain intact.

3.4. Possible origin of annealing peak, T_a

A linear line with a slope of unity is found between T_a and T_c, and T_a is always ca. 4.0 ± 0.3 °C above T_c. Up to now, no report has been presented in the literature for the appearance of T_a in the sPS samples. However, the presence of annealing peak has been described in some details for certain semi-stiff polymers, such as iPS [39–42], poly(ether ether ketone) [43], and poly(ethylene terephthalate) [44]. One hypothesis for T_a is ascribed to the presence of the rigid amorphous phase existing between the mobile amorphous phase and the crystalline lamellar phase. Based on the TEM observations, Liu et al. [39,40] showed no morphological variation by holding iPS samples at a temperature slightly higher than T_a for a short time. They concluded that the annealing peak is not associated with the melting of subsidiary crystals but resulted from the nonreversible relaxation process of rigid amorphous phase. Xu et al. [41] made a similar conclusion on the basis of their

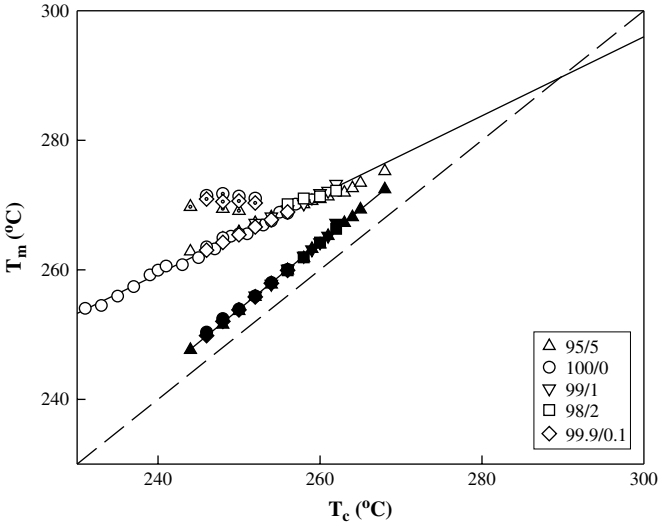

Fig. 11. Determination of equilibrium melting temperature of sPS/CNC composites by Hoffman–Weeks plot. (Filled symbols for T_a, open symbols for T_{ml}, and open symbols with a dot center for T_{mh}. All the samples are crystallized in the β form).

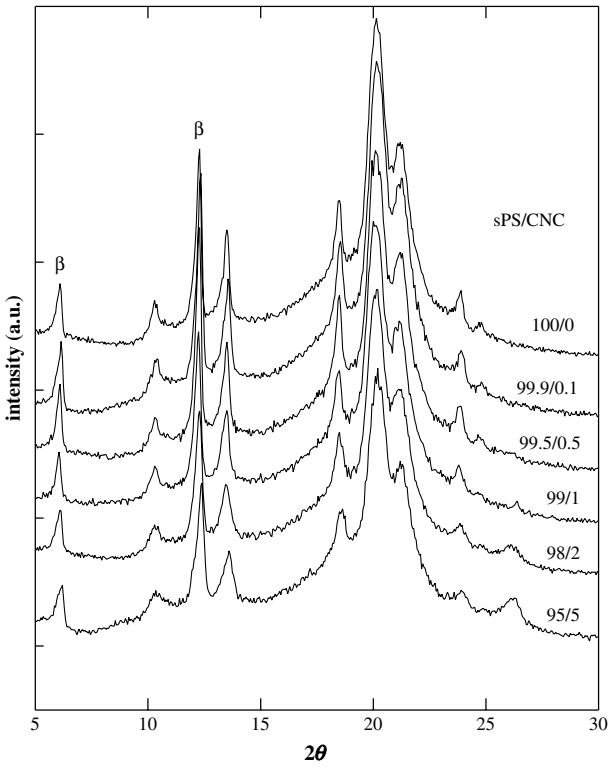

Fig. 12. WAXD intensity profiles of the sPS/CNC composites melt-crystallized isothermally at 260 °C. The typical β-form diffraction peaks at $2\theta \sim 6.13°$ and 12.3° are indicated. The small peak at $2\theta \sim 26.1°$ is associated with the (002) plane of CNC, in the presence of graphitic structure.

FTIR results. They showed no detectable spectrum difference of the crystallite-related absorbance prior to and post to the heating of crystallized samples to a temperature higher than T_a. In contrast, Duan et al. [42] recently carried out in situ FTIR measurements on the iPS samples and provided a different hypothesis that T_a is attributed to the relaxing of ordered 3_1 helix chains (sequence length of 10) in the amorphous phase. Another plausible source is the melting of micro-crystallites developed upon long-time annealing. On studying the melting of polyethylene with sufficient branching content, similar annealing peak is also observed [45,46] and is considered to the formation of fringed-micellar or chain cluster structures developed in the constrained environments between lamellae [45].

As the sizes of CNC primary particles or aggregates (50–400 nm) are much larger than the lamellar thickness (~7.2 nm, as illustrated later), the growth of sPS lamellae between CNC particles is not only restricted in its lateral direction but also the chain-folding direction, especially in the highly filled composites. Therefore, the number of lamellae in each lamellar stack is lowered and some amorphous pockets are formed at the impingement of growing lamellar stacks. It is likely for some imperfect micro-crystals to reside in these amorphous pockets and be melted away during heating at T_a. On the other hand, it seems more unlikely that its origin is associated with the enthalpy relaxation of the rigid amorphous phase because T_a is significantly higher than T_g (~96 °C).

The multiple-melting behavior of sPS/CNC composites (Fig. 10a) did not result from the polymorphism of sPS because only β-form is detected by FTIR and WAXD. On the basis of morphological observations, lamellar insertion model was verified along with the re-crystallization model to account for the double-melting behavior of neat β′-form sPS [47]. In other words, the position of the T_{mh} is dependent upon the average thickness of the un-melted lamellae as well as the thickened ones relevant with the re-crystallization process. Thus, T_{ml} is more representative than T_{mh} to be used to determine to T_m^0 by the Hoffman–Weeks plot. According to the T_{ml}–T_c plot, the determined T_m^0 is ca. 289.7 °C and the thickening coefficient is 1.64 for the neat sPS as well as the CNC-filled composites. The derived T_m^0 is in good agreement with that which has been reported previously [7]. In addition, the T_{mh} is at 270.6 ± 0.8 °C and it is absent for samples crystallized at T_c higher than 252 °C.

3.5. Lamellar morphologies of sPS

To study the CNC effects on the lamellar morphologies, a detailed study has been carried out for sPS/CNC composites melt-crystallized at 260 °C. Fig. 12 shows their WAXD intensity profiles; the appearance of characteristic diffraction peaks for the β-form crystals at $2\theta = 6.13°$ and 12.3° is obvious. According to previous classification [6], it can be further characterized as β′-form sPS due to its less order structure, giving additional diffraction peaks at 10.5°, 13.6° and 18.5°, respectively. In addition to diffraction peaks relevant with β′-form crystals, a small peak at 26.1° is also detected for the sPS/CNC composites. This is associated with the (002) *d*-spacing of CNCs possessing the graphitic structure [2]. After de-convolution of the diffraction curves, the crystallinity fraction (φ^{WAXD}) is then estimated from the ratio of integrated intensities from all the crystalline peaks to the total intensity curve. For these isothermally crystallized composites, the crystallizability of sPS chains is found to be reduced for the sample with ϕ_{CNC} larger than 1% (Table 2). This is similar with the results obtained from the non-isothermal crystallization (Table 1). The morphological features of

Table 2
Crystallinity, lamellar thickness, and thermal properties of sPS/CNC composites melt-crystallized at 260 °C.

sPS/CNC	$\varphi^{WAXD}/(1-\phi_{CNC})$	l_c (nm)	T_m (°C)	T_d (°C)
100/0	0.395	7.4 ± 1.5	269.6	386.7
99.9/0.1	0.407	7.2 ± 1.2	271.1	391.8
99.5/0.5	0.391	6.7 ± 1.3	269.7	390.7
99/1	0.355	7.4 ± 1.6	269.4	396.6
98/2	0.345	6.8 ± 1.3	272.2	397.5
95/5	0.329	7.9 ± 1.4	269.4	406.4

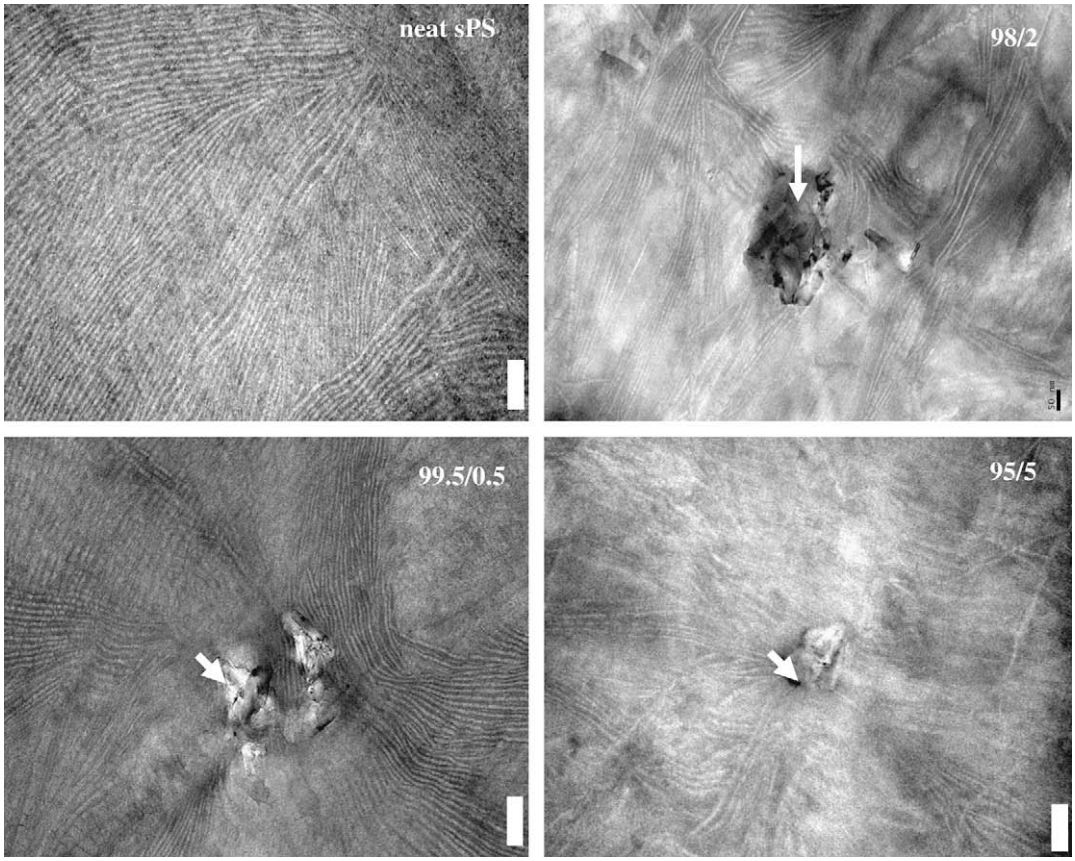

Fig. 13. TEM micrographs of sPS/CNC composites. The scale bar is 100 nm and the arrows point out the location of CNCs.

sPS/CNC composites obtained by TEM are shown in Fig. 13. As expected, neat sPS exhibits an ordered lamellar morphology. This morphology persists qualitatively in composites with lower CNC contents (99.9/0.1 and 99.5/0.5 samples). Higher loading of CNCs leads to the randomly oriented lamellar stacks with reduced lateral dimensions. Some large amorphous pockets can be readily observed at the impingement of the growing lamellar stacks. It is proposed that some crystallizable sPS chains (or segments) may be trapped in these lamella-free pockets due to the overwhelming primary nucleation. Likewise, they have difficulties in forming a new lamella due to the constraints from the neighboring lamellae. In spite of the restricted mobility resulting from the geometrical confinements, these trapped sPS chains (or segments) may undergo short range motion to develop a less perfect crystallite like an aggregate of chains having certain level of crystallographic packing in directions parallel and perpendicular to the chain axis. These fringe-miscelle-like micro-crystals may not be readily detected by the WAXD and TEM due to its imperfect structure. However, DSC is sensitive enough to trace its melting by the appearance of the small annealing peak at T_a.

Based on the TEM micrographs shown in Fig. 13, the average lamellar thickness, l_c, was obtained from a collection of ~300 lamella population and the results are also tabulated in Table 2. This was in conjunction with their corresponding melting temperature determined from DSC heating scan. It is of significance to note that l_c remains unchanged (~7.2 nm) regardless of the CNC content. A slight variation of T_m is observed but the CNC effect is marginal. This is in a fair agreement with the l_c results. TGA was performed on composites to investigate the CNC effects on the thermal stability of the sPS matrix. The resulting curves are shown in Fig. 14. For the neat CNCs, two-stage weight loss is observed from the TGA curve (not shown). A relatively fast degradation is first seen at 200 °C until 320 °C, where a mild degradation is followed up to a temperature of 800 °C. It should be noted that the first stage involves with the degradation of the –COOH functional groups on the surface-treated CNC, and about 82 wt% of CNC is remained at 800 °C. For the composites, the weights remaining at 500 °C are almost entirely due to the remaining CNCs and its amount is consistent with the initial CNC loading. The temperatures at 5% weight loss, T_d, are determined from the curves and are displayed in

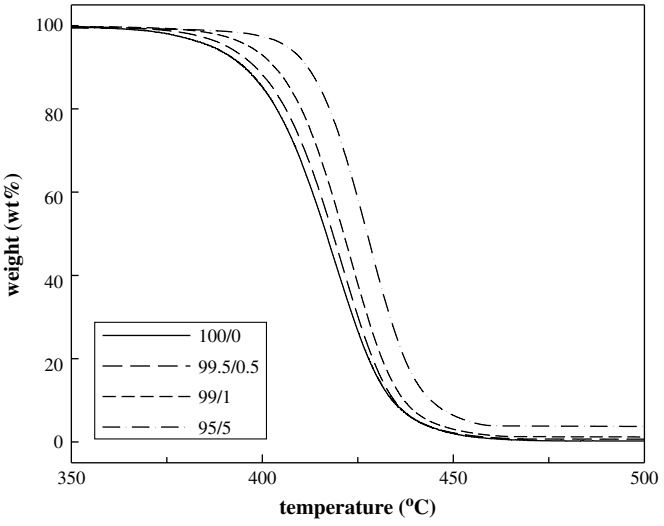

Fig. 14. TGA curves of sPS/CNC composites.

Table 2 as well. The retardation of sPS decomposition is evident due to the presence of CNCs; a maximum increase of 20 °C in T_d is observed for composites with CNCs of 5 wt%. The retardation is likely to be a result of adsorption, by the activated CNC surface, of free radicals generated during sPS decomposition.

4. Conclusions

The addition of CNC into sPS samples showed a negligible effect on the glass transition and equilibrium melting temperature of the as-formed composites. Isothermal and non-isothermal crystallization of sPS/CNC composites have been investigated by means of DSC. The corresponding results showed that CNC addition gave rise to a fast crystallization of sPS induced either from the melt-quenched or from the molten state. As supported by PLM observations, with increasing CNC concentration the micron-scaled spherulites became smaller, and a negligible change in the crystal growth rate was found. Thus, it is concluded that the enhanced sPS crystallization is attributed to the existence of profound primary nucleation density. CNC addition also resulted in the formation of less parallel lamellae of sPS with a short lateral dimension but intact lamellar thickness. Thereby, it gives similar melting temperatures regardless of the CNC content. In conclusion, CNCs are verified to be an excellent nucleating agent for accelerating the crystallization of sPS and promote its thermal stability at high temperatures.

Acknowledgments

The authors are grateful to the National Science Council of Taiwan (ROC) for the research grant (NSC94-2216-E-006-004) that supported this work. We also thank ITRI for providing us the surface-modified CNCs and CNTs. Financial support from the "Landmark Program" of the NCKU top University Project (#B0147) to purchase the FTIR Spectrum 100 is acknowledged with gratitude.

References

[1] Moniruzzaman M, Winey KI. Macromolecules 2006;39:5194.
[2] Han S, Yun Y, Park KW, Sung YE, Hyeon T. Adv Mater 2003;15:1922.
[3] Hwang GL. Japanese patent JP 20,030,910; 2003.
[4] Zeng H, Zhu L, Hao G, Sheng R. Carbon 1998;36:259.
[5] Lin TC, Li YY. Carbon 2006;44:2045.
[6] Guerra G, Vitagliano VM, De Rosa C, Petraccone V, Corradina P. Macromolecules 1990;23:1539.
[7] Woo EM, Sun YS, Yang CP. Prog Polym Sci 2001;26:945.
[8] De Rosa C, De Ballesteros OR, Di Gennaro M, Auriemma F. Polymer 2003;44:1861.
[9] De Rosa C. Macromolecules 1996;29:8460.
[10] Cartier L, Okihara T, Lotz B. Macromolecules 1998;31:3303.
[11] De Rosa C, Rapacciuolo M, Guerra G, Petraccone V, Corradini P. Polymer 1992;33:1423.
[12] Chatani Y, Shimane Y, Ijitsu T, Yukinari T. Polymer 1993;34:1625.
[13] De Rosa C, Guerra G, Petraccone V, Pirozzi B. Macromolecules 1997;30:4147.
[14] Chatani Y, Shimane Y, Inagaki T, Ijitsu T, Yukinari T, Shikuma H. Polymer 1993;34:1620.
[15] Gowd EB, Nair SS, Ramesh C, Tashiro K. Macromolecules 2003;36:7388.
[16] Wu HD, Wu ID, Chang FC. Macromolecules 2000;33:8915.
[17] Haggenmueller R, Fischer JE, Winey KI. Macromolecules 2006;39:2964.
[18] Uehara H, Kato K, Kakiage M, Yamanobe T, Komoto T. J Phys Chem 2007; 111:18950.
[19] Li L, Li CY, Ni C. J Am Chem Soc 2006;128:1692.
[20] Grady BP, Pompeo F, Shambaugh RL, Resasco DE. J Phys Chem B 2002;106:5852.
[21] Bhattacharyya AR, Sreekumar TV, Liu T, Kumar S, Ericson LM, Hauge RH, et al. Polymer 2003;44:2373.
[22] López Manchado MA, Valentini L, Biagiotti J, Kenny JM. Carbon 2005;43:1499.
[23] Xu D, Wang Z. Polymer 2008;49:330.
[24] Gorrasi G, Romeo V, Sannino D, Sarno M, Ciambelli P, Vittoria V, et al. Nanotechnology 2007;18:275703.
[25] Zhang S, Minus ML, Zhu L, Wong CP, Kumar S. Polymer 2008;49:1356.
[26] Minus ML, Chae HG, Kumar S. Polymer 2006;47:3705.
[27] Shieh YT, Liu GL, Hwang KC, Chen CC. Polymer 2005;46:10945.
[28] Manfredi C, De Rosa C, Guerra G, Rapacciuolo M, Auriemma F, Corradini P. Macromol Chem Phys 1995;196:2795.
[29] Lu M, Zhou W, Mai K. Polymer 2006;47:1661.
[30] Wu HD, Tseng CR, Chang FC. Macromolecules 2001;34:2992.
[31] Wang ZM, Chung TC, Gilman JW, Manias E. J Polym Sci Polym Phys 2003; 41:3173.
[32] Woo EM, Wu FS. J Polym Sci Polym Phys 1998;36:2725.
[33] Chiu FC, Li MT. Polymer 2003;44:8013.
[34] Guerra G, De Rosa C, Vitagliano VM, Petraccone V, Corradini P. J Polym Sci Polym Phys 1991;29:265.
[35] Wang C, Wang ML, Fan YD. Macromol Chem Phys 2005;206:1791.
[36] Balberg I. Philos Magn B 1987;56:991.
[37] Wu TM, Hsu SF, Chien CF, Wu JY. Polym Sci Eng 2004;44:2288.
[38] Hoffman JD, Weeks JJ. J Res Natl Bur Stand A 1962;66:13.
[39] Liu T, Petermann J, He C, Liu Z, Chung T-S. Macromolecules 2001;34:4305.
[40] Liu T, Petermann J. Polymer 2001;42:6453.
[41] Xu H, Ince BS, Cebe P. J Polym Sci Polym Phys 2003;41:3026.
[42] Duan Y, Zhang J, Shen D, Yan S. Macromolecules 2003;36:4874.
[43] Lee Y, Porter RS. Macromolecules 1987;20:1336.
[44] Holdsworth P, Turner-Jones A. Polymer 1971;12:195.
[45] Alizadeh A, Richardson L, Xu J, McCartney S, Marand H, Cheung YW, et al. Macromolecules 1999;32:6221.
[46] Wang C, Chu MC, Lin TL, Lai SM, Shih HH, Yang JC. Polymer 2001;42:1733.
[47] Wang C, Huang CL, Cheng YW, Chen YC, Shong J. Polymer 2007;48:7393.